Prepared for submission to JCAP

arXiv:1405.6725v1 [astro-ph.CO] 26 May 2014

Particle ejection during mergers of dark matter halos

Isabella P. Carucci,[1] **Martin Sparre,**[1] **Steen H. Hansen,**[1] **and Michael Joyce**[2]

[1]Dark Cosmology Centre, Niels Bohr Institute,
University of Copenhagen, Juliane Maries Vej 30, 2100 Copenhagen, Denmark
[2]Laboratoire de Physique Nucléaire et Hautes Énergies,
Université Pierre et Marie Curie - Paris 6, CNRS IN2P3 UMR 7585,
4 Place Jussieu, 75752 Paris Cedex 05, France

Abstract. Dark matter halos are built from accretion and merging. During merging some of the dark matter particles may be ejecteted with velocities higher than the escape velocity. We use both N-body simulations and single-particle smooth-field simulations to demonstrate that rapid changes to the mean field potential are responsible for such ejection, and in particular that dynamical friction plays no significant role in it. Studying a range of minor mergers, we find that typically between $5-15\%$ of the particles from the smaller of the two merging structures are ejected. We also find that the ejected particles originate essentially from the small halo, and more specifically are particles in the small halo which pass later through the region in which the merging occurs.

Keywords: dark matter: halos, techniques: numerical

Contents

1 Introduction **1**

2 N-body simulations **3**
2.1 Simulation setup 3
2.2 Results 4
2.2.1 Identifying the ejected particles 4
2.2.2 Numerical tests 4
2.2.3 Which particles are ejected? 5
2.2.4 Analysis of particle energies 7
2.2.5 Mechanism of ejection 7
2.2.6 What determines the fraction of ejected particles? 9

3 Tracing particles in an analytical potential **9**
3.1 Simulation Set-Up 10
3.2 Particle trajectories 12
3.3 Fraction of ejected particles 14

4 The relation between scale radius and fraction of ejected particles **14**

5 Discussion and Conclusion **16**

1 Introduction

Observations suggest that structure formation in the Universe proceeds hierarchically, with the smallest structures collapsing first and then later merging to form larger structures. An important property of mergers is that if two halos with identical density profiles merge, the merger remnant will have a density profile with the same inner and outer slopes as the initial profiles [1]. It has been proposed that this behaviour may be understood from considerations about mixing of collisionless systems [2]. Further merger remnants have been found to be triaxial with a major axis along the collision axis [3], and the velocity anisotropy profiles are typically radial, in the sense $\sigma_{\rm r}^2 \geq \sigma_{\rm tan}^2$, whether calculated in spherical or elliptical bins. The velocity anisotropy profiles of merger remnants are, however, not simple functions; they are asymmetric in the sense that a very different behaviour is seen along different axes [4]. It has been pointed out [5] that the velocity ellipsoids of a halo are typically aligned with the major axis, and it means that the velocity anisotropy parameter gives a misleading description of triaxial halos.

The relaxation and mixing processes in collisionless mergers have been examined in [6], where it was found that mixing of the 6-dimensional phase space distribution function mainly occurs during the tidal shocking arising when the center of the merging halos pass through each other, and that about 40 % of the particles from the merging halos are located outside the virial radius of the remnant. In controlled numerical galaxy collisions it has been known for a long time that some particles are ejected with positive energies (see e.g. [7]). In cosmological simulations it has been found that unbound particles are abundant in halos which have recently undergone a major merger [8].

Why particles are ejected in the course of a merger is straightforward to understand on energetic grounds. When a small structure is engulfed by a larger one, it will be ripped apart dynamically, and a new equilibrium state will be reached. At the end of this equilibration, the virial theorem must hold for the bound particles, i.e.,

$$2K + W = 0\,, \tag{1.1}$$

where K and W are the total kinetic and potential energy of the bound particles (with K calculated relative to their centre of mass). The total energy of the virialized particles is thus $E_b = -K$. For the case of two virialized structures initially very far from one another, the total energy can be written as $E = -K_1 - K_2 + K_{CM}$ where K_1 and K_2 are the initial kinetic energies of the two systems (relative to their centre of masses) and K_{CM} is the kinetic energy of the centre of masses of the two halos when they are far apart. By energy conservation we therefore have that particles must be ejected if K_{CM} in the centre of mass frame, i.e., the kinetic energy of the initial relative motion, is sufficiently large to make the total initial energy positive: dark matter, unlike baryons which can radiate, have no other way of discarding the excess energy in the system. In the case of cold dark matter, such relative motion is typically small, and we will in fact assume it to be zero, i.e., the structures start far apart without initial relative motion. In this case, from a global energetic point of view, ejection *may or may not* take place. However, in the case of a small structure which encounters a very large structure it is not difficult to see why such ejection *does* in fact typically take place, and why the ejected particles are (as we will verify in detail below) those in the small structure. Neglecting completely the potential energy due to the small structure, we can consider the particles belonging to it as unbound particles falling into the fixed potential of the large structure. The condition of virialization in this fixed potential then imposes that energy must be ejected: for example, if two particles arrive from far away with zero energy, and virialize in this way, the combination of the virial condition and energy conservation would then give $2(K + k_a + k_b) + (W + w_a + w_b) = k_a + k_b = 0$, where k_a (w_a) and k_b (w_b) are the average kinetic (potential) energies of the particles, a condition which cannot be satisfied. The system, however, can reach a virial equilibrium without any signification modification of the large structure by ejecting particles carrying away excess energy. From a dynamical point of view, the particles in the small structure are much less bound and the potential fluctuations induced by the merger are of order the initial potential energy of this structure, precisely of the order required to eject them.

In this paper we perform numerical simulations to study and characterize the ejection of particles in mergers and to understand the mechanism responsible for this ejection. We use N-body simulations to study the ejection of particles in minor mergers, and we use single particle simulations in smooth potentials to demonstrate that the ejection mechanism is indeed a mean-field effect. Particle (and energy) ejection during the process of violent relaxation has been previously discussed at length in [9], and studied in detail with N-body simulations for the case of cold quasi-spherical initial conditions. Typically about 15% of the particles are found to ejected in this case, and it is shown that these are particles initially in the outer shells which "arrive late" at turnaround and pick up a positive energy kick as they travel in the potential sourced by the re-expanding potential of the bulk of the particles. Despite the quite different initial conditions studied here, we will see that the mechanisms at play in the ejection are in fact very similar.

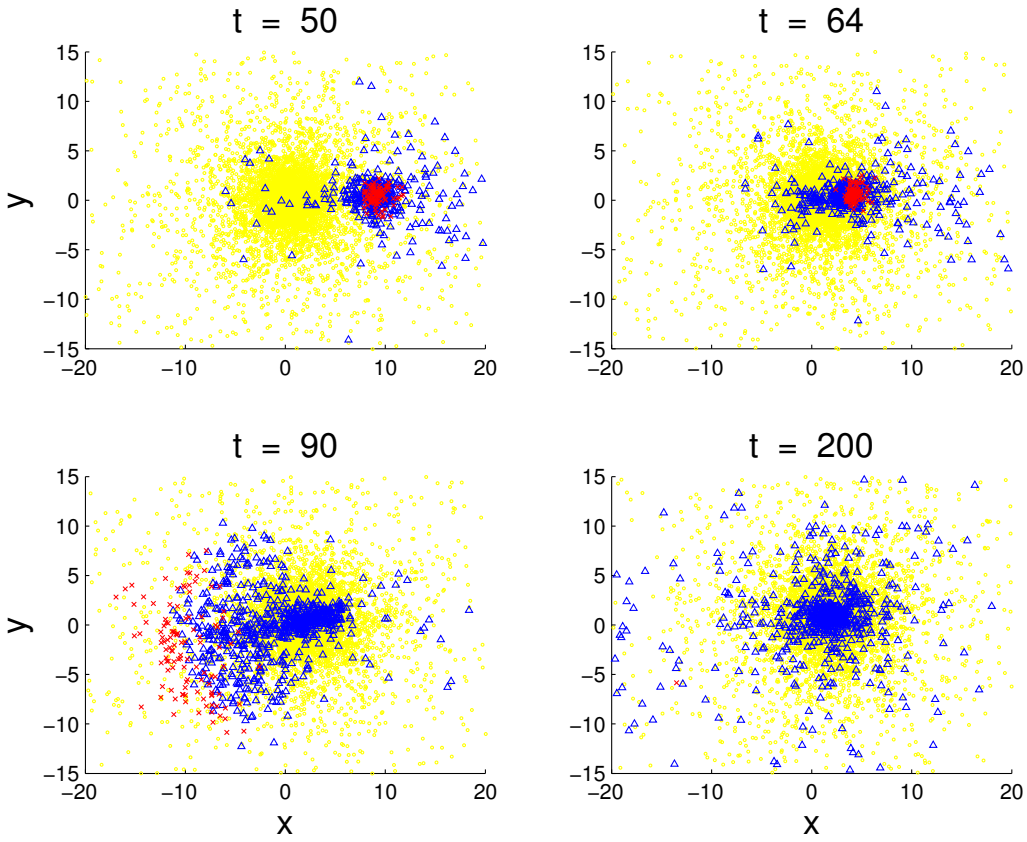

Figure 1. The positions in x and y of the particles at different time steps of the simulation. The yellow dots are particles belonging to the major halo, the blue triangles are the minor halo particles that stays bound throughout the simulation, and the red stars are the particles which get ejected. At $t = 64$, it can be seen that the ejected particles from the minor halo arrive at the plane of the center of the major halo slightly later than the center of the minor halo does.

2 N-body simulations

In this section we will describe our N-body simulations of minor mergers, which have been performed using the `GADGET-2` code [10, 11]. All the simulations were pure dark matter simulations, where dark matter is modelled as collisionless particles, and in a non-expanding universe with open boundary conditions.

2.1 Simulation setup

We study mergers between halos with a mass ratio of 1:10, representative of typical mergers encountered in cosmological simulations. In our simulations we have 10^5 particles in the big halo and 10^4 particles in the small halo. We work in units in which the gravitational constant G is unity. Further we take both the mass of the larger halo, M_1, and its scale radius, r_s, to be unity. All particles have the same mass. We use a gravitational softening given by 0.023 in the `GADGET-2` parameter file, and force and time integration accuracies are fixed by `ErrTolForceAcc` $= 0.005$ and `ErrTolIntAccuracy` $= 0.025$, respectively. We will discuss further below tests we have performed on the stability of our results to variation of these parameters.

The positions and the velocities of the particles are chosen so that each structure, treated as an isolated system, is in a steady state in virial equilibrium. Positions are assigned from the Hernquist mass profile [12],

$$\rho(r) = \frac{1}{r/r_{\rm s}} \frac{\rho_0}{(1 + r/r_{\rm s})^3},$$

and the velocities are selected from a Gaussian PDF with the initial isotropic velocity dispersion derived from the Jeans equation. The initial velocities are truncated at $0.95 v_{\rm esc}$. We ran simulations with different scale lengths, r_{s2}, of the small halo (but with fixed mass).

The centres of mass of the two halos are placed at $y = 0$ and $z = 0$ in our cartesian coordinate system. Instead in the x direction we place the big halo at 0 and the small at 15. The latter value is a rough estimate for the turnaround radius of the big structure [13, 14], assuming it to have a typical concentration of galaxies [15]. Having chosen to place the minor halo at the turnaround radius of the major, we start the simulation start with both halos at rest. The small structure starts approaching the big one, pulled by its gravitational attraction. After the merger we continue the simulation for at least 10 more dynamical times, where we define a typical dynamical time from the circular velocity at $r_4 = 4\, r_{s1}$, $\tau_{\rm dyn} = r_4/v_c(r_4)$. When we observe that the total energy of the new structure (without the ejected particles) is constant, we deduce the system has reached a new equilibrium.

2.2 Results

2.2.1 Identifying the ejected particles

Our first simulation uses a scale radius $r_{s2} = 0.3$ for the small halo. The positions of the particles as a function of time is shown in figure 1. The red stars in the plot are particles which start in the minor halo and are ejected during the simulation, where we label a particle *ejected* if its total energy in the final snap-shot is positive.

The colour code allows us to follow the ejected particles in red from the beginning of the run, to distinguish them from the other particles belonging initially to the small structure, in blue, and those belonging to the big structure, in yellow. We see that, at $t = 50$, the small halo has not yet crossed the big halo core and the red particles are well mixed with the blue ones. As the small halo enters the large halo's core at $t = 64$, we see that the red particles are those which "lag behind"and are the last ones to cross the core. The next snapshot describes the subsequent ejection, and in the last one at $t = 200$ (~ 23 dynamical times) there are no longer red particles within 15 times the scale radius.

2.2.2 Numerical tests

As pointed out in the introduction, we expect ejection to happen generically in this kind of merger. Nevertheless to check that the mass ejection we observe numerically is not the consequence of some other effect, notably ill-posed initial conditions (i.e. particles not in equilibrium to begin with), or accumulated integration errors in the particle orbits, we run additional specific test simulations.

We test first that our results are insensitive to the use of the Gaussian approximation of the initial velocities. Specifically, we use the Eddington inversion method [16] to set up initial equilibrated structures (using an implementation which was tested in [17, 18]), and we find that merger time and number of particles ejected are identical within a few percent. Also the interesting feature of figure 1, that the ejected particles are the ones arriving "late" is exactly the same for initial structures created using the Eddington method.

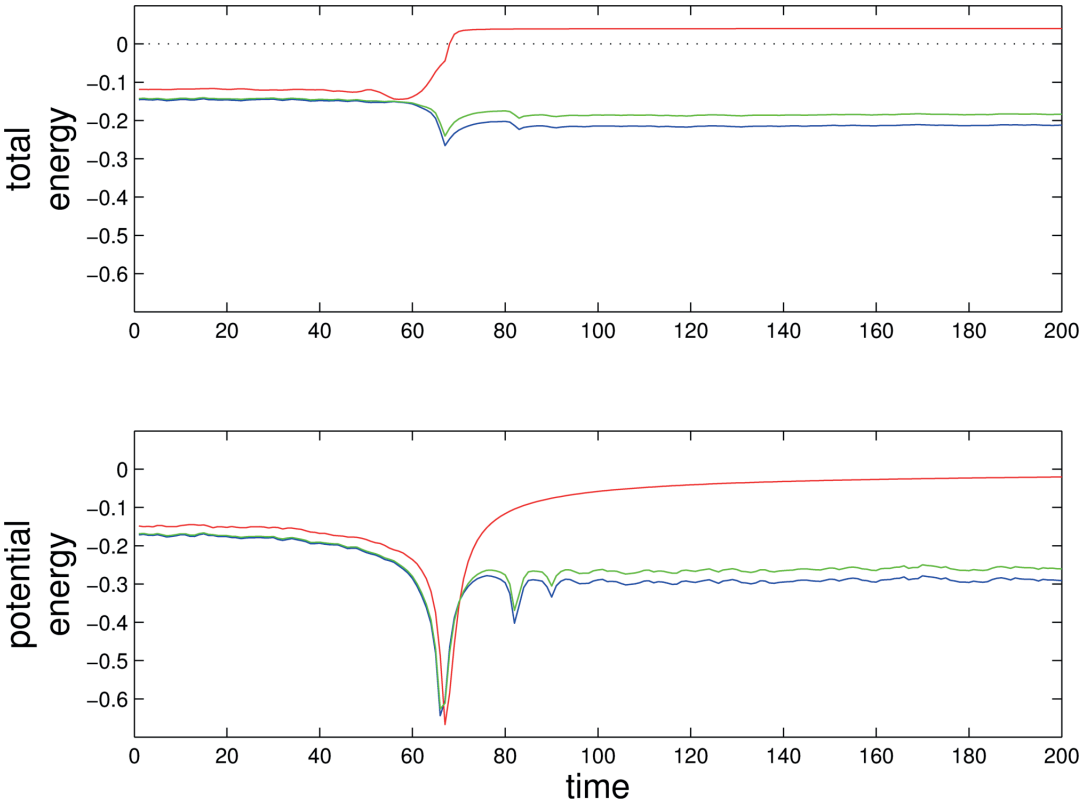

Figure 2. Time evolution of the total energy (upper panel) and potential energy (lower panel) of all the particles belonging to the small halo (green), of the particles which remain bounded (blue), and of those which are ejected (red).

Figure 1 keeps its characteristics also when we run more accurate simulations, taking `ErrTolForceAcc` $= 0.001$ and `ErrTolIntAccuracy` $= 0.005$ (i.e. a factor of five smaller than in our fiducial simulations). In this case too, merger time and number of particles ejected are stable within a few percent.

2.2.3 Which particles are ejected?

The mechanism of ejection is in fact simply that of violent relaxation in general, as originally described by [19] for stellar systems: starting from an initial configuration which is far from dynamical equilibrium, such a system can relax precisely because, in the time dependent gravitational potential, particles' energies can change rapidly (i.e. on mean field time scales). If the fluctuations of potential are sufficiently violent, particles can reach and surpass the escape velocity of the system.

More specifically it is the particles that just happen to arrive later in the region at the centre of the merger which pick up a large positive kick to their energy in a short time as they pass through the time-dependent potential well created by the rest of the mass. To see that this is the case, we plot in the lower panel of figure 2 the average potential energy of the blue (bounded) and red (escaping) particles as defined in the previous figure, as well as the average over all particles (in green). It can be seen clearly that the red particles pass on average through the minimum of the potential well slightly later than the blue ones.

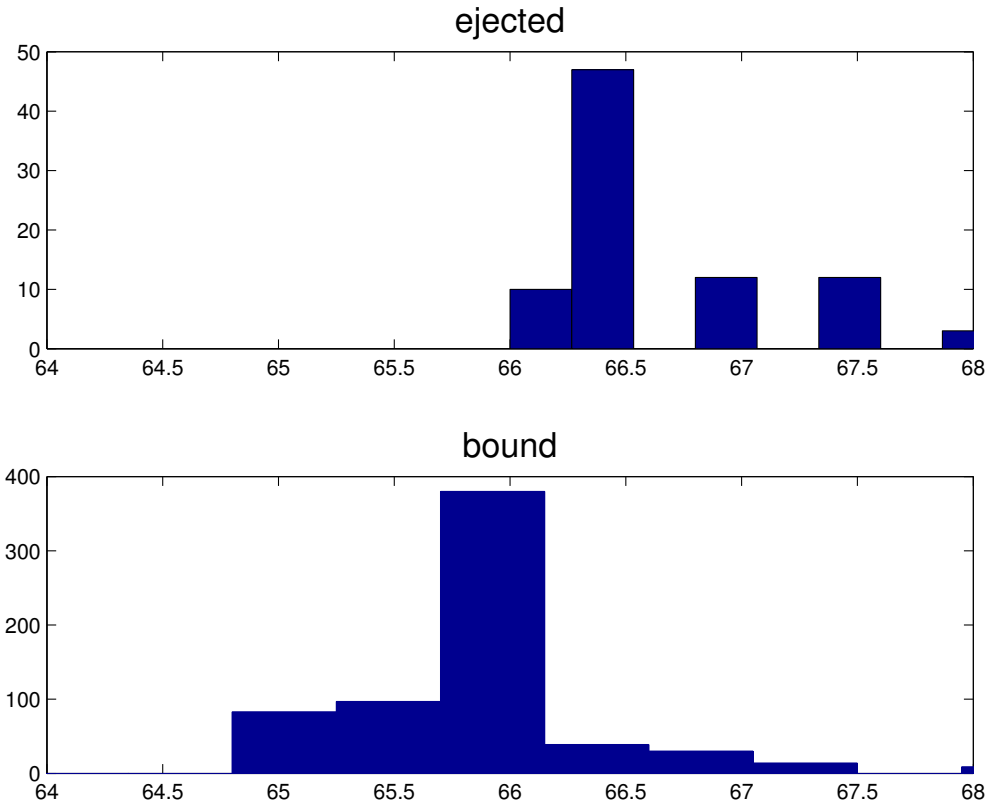

Figure 3. The distribution of "dip-times" for all the particles which are either ejected or bound. The dip-time is defined as the time when the potential energy of the particle reaches its minimum. The particles which are ejected are seen statistically to have a later dip-time than the particles which are bound.

Further from the plot in the upper right panel of figure 1, it can be seen that all the ejected particles were on the right side of the minor halo at $t = 64$.

In order to show that the ejected particles are the late arrivers, we follow the orbit of each particle from the small halo, and we find the time when the potential energy is at a minimum for each particle. For this figure we include only particles inside 5 times the scale radius. We can now plot the distribution of these "dip-in-energy" times for the particles which will eventually be ejected, and compare this to the particles which will be bound, and we clearly see the difference in Figure 3. We see that the peak of the ejected particles is later than the peak for the particles which remain bound.

In figure 4 we plot the radial velocities and the radii of the particles in the small halo before the merger happens, for two different values of r_s. The red circles label the particles that will subsequently be ejected. They are distributed almost as the other particles: in the sense that at any given radius the velocity distribution of the ejected particles is similar to that of the particles which remain bound. Furthermore, the ejected particles are neither the most energetic nor those furthest from the centre of the structure. They are not, on the other hand, not the particles orbiting at the smallest radii, and hence not the most bound particles. Further plotting other quantities such as the angular momentum (modulus and direction) we have not identified any particular feature that characterises the particles in question. The decisive factor thus seems to be whether or not a particle is falling early or

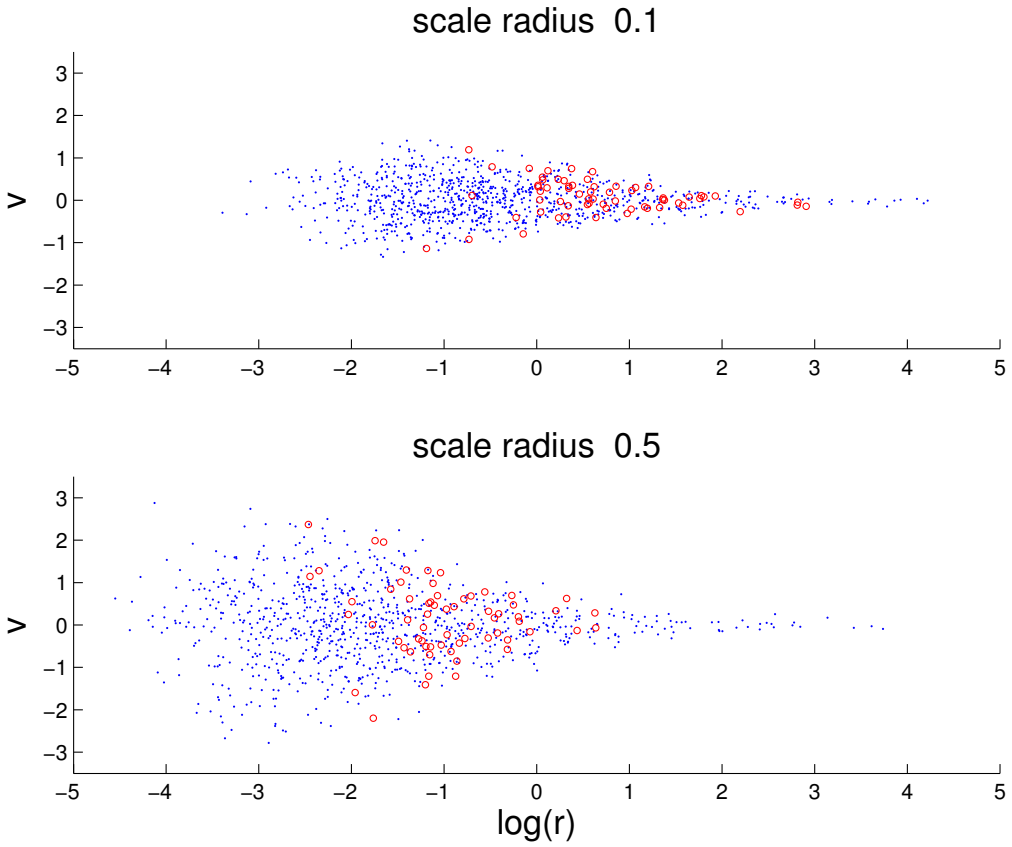

Figure 4. Radius r and radial velocity v normalised with the related virial quantities for 2 different scale radii for the small structure. The red circles represent the particles which will later be ejected, the blue dots are the particles which remain bound.

late into the combined potential of the cores of the halos.

2.2.4 Analysis of particle energies

The particles which are ejected are those of which the energy is positive after the merger. Figure 5 shows the evolution of the energy of a few randomly selected particles. In the case of the big structure, its particles' energies stay roughly constant in a range of values well represented by the total energy of the halo averaged over the number of its particles. None of the particles from the big halo are ejected during the merger. Among the chosen particles belonging to the small halo, there are a couple for which the total energy becomes positive after the merger, roughly in a time window between $t = 60$ and $t = 70$. None of the particles are ejected before $t = 50$. The mean particle energy of the small halo displays a sharp peak at the moment of the merger and then falls back to a roughly constant value, which is higher than the initial one. Thus, during a collision in this simulation 11% of the particles from the small halo are freed from the system during the merger, and will never return.

2.2.5 Mechanism of ejection

The observation that it is the particles coming in later which are ejected is similar to the case of cold uniform spherical collapse in [9, 22], where the ejected particles were found to

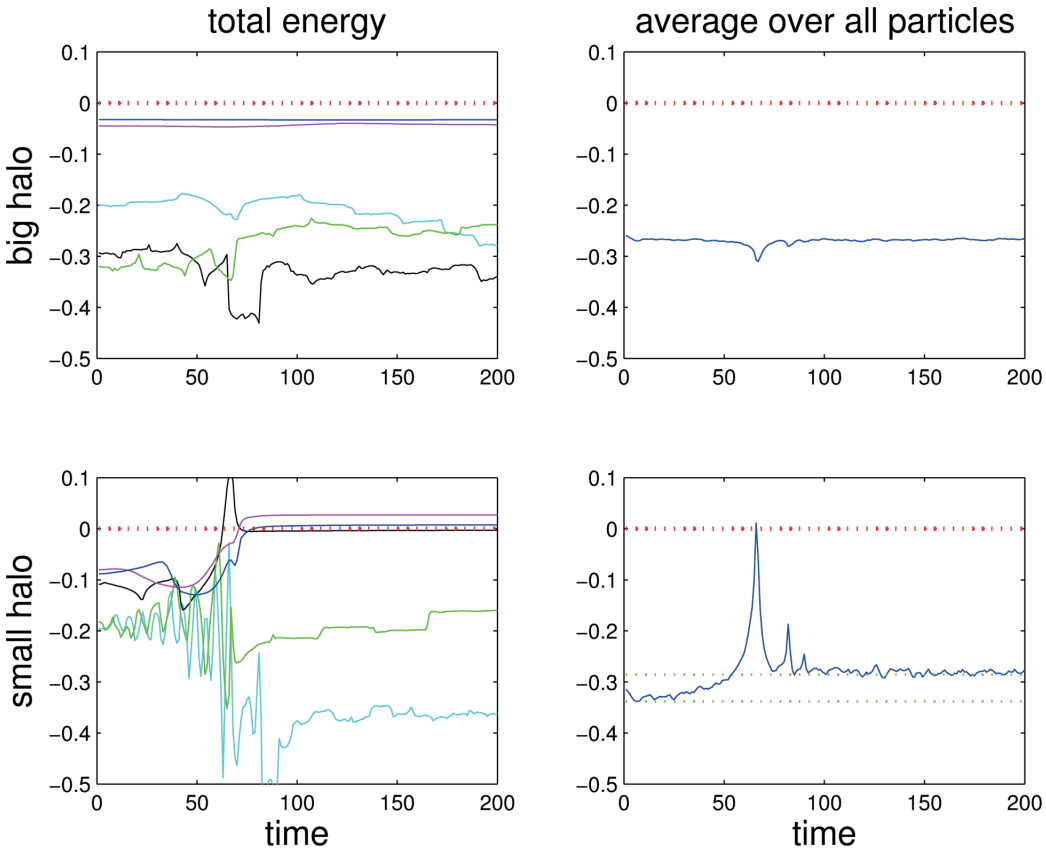

Figure 5. Time variation of the total energy. On the left we see the time evolution of five different particles, and on the right the average over all the particles. The upper plots are for the big halo, the lower ones for the small halo. The red dotted line shows the zero point of the energy.

be those starting out in the outer shells. In this case close analysis of the particle energies shows that those which escape pick up the energy leading to their ejection when they pass through the potential generated by the bulk of the mass which has already turned around and starting re-expanding: as the time derivative of the potential is then positive, they gain energy.

A detailed view of the time evolution of particle energies here reveals that what is happening in the minor merger is very similar. In figure 6 we zoom in on the time steps during the merging of the small structure. We follow again the evolution of five particles, where the green and red (dashed lines) are ejected particles, whereas the blue and purple (dotted lines) are finally bounded. Further we show the energy of the most bound particle from the small structure (stars), and the same from the big structure (triangles). Inspecting the time steps between 62 and 67, we see that the potential of both the small and the large structures get deeper. This is natural because during the first passage when the 2 structures overlap for the first time, the potentials deepen. However, during the time-steps from 67 to 70 the potential falls back to a smaller absolute value. This is just after the first passage of the small structure. After this point, the potential flattens out close to the final value.

Now, comparing the time of passage of the particles which will remain bounded (black and purple dots), we see that they pass the center during the deepening of the potential of the structure. The particles which are ejected, on the other hand, arrive later, during the

phase when the potential happens to be weakening (i.e. increasing towards less negative values). As the sign of the time derivative of the mean field potential is positive the energy of the particles increase, since the time variation in particle energy along a trajectory is equal to the time derivative of potential energy [19], $dE/dt = \partial\Phi/\partial t$.

While we have shown here the time evolution of only two ejected particles, we underline that figure 1 shows that of the roughly 1000 ejected particles, essentially all of which arrive late during the merger as we have described. We note that this effect is analogous to the so-called late-time integrated Sachs-Wolfe effect, in which photons gain energy because of the decay of the potential they are traversing.

We note that temporal variation of the mean field potential is indeed well known to induce changes in the energy of individual particles, potentially even leading to evaporation of particles, e.g. discussed as tidal forces [20], and as gravitational shocks during merging [21]. Very large changes in energy are also known to occur during impulsive tidal shocking [6] which exactly happens during pericenter passages.

Whereas these previous studies have considered average changes in energy, we emphasize here that , like in the case of spherical cold collapse [9], the particles which pick up enough energy to be ejected are those specific ones which arrive late relative to the time at which the total potential reaches its minimum. These particles are thus ejected because of a coincidence between their individual orbits combined with the potential changes during merging.

2.2.6 What determines the fraction of ejected particles?

After having considered the phenomenon of ejected particles in mergers, we proceed by performing simulations with different sizes of the minor halo. We run different simulations keeping the scale radius of the big halo set to $r_{\rm s} = 1$, while changing the small halo $r_{\rm s}$ within the range $0.1 \leq r_{s2} \leq 0.7$. The ratio of the halo masses is unchanged (equal to 0.1).

In figure 7 we plot the fraction of the minor halo particles that get ejected for the different values of the minor halo's scale radius. We see that the number of ejected particles grows with the dynamical time up to a peak that corresponds roughly to a small structure with a dynamical time $t_{\rm dyn}({\rm small}) \simeq 0.7 t_{\rm dyn}({\rm big})$, and then beyond this point the number decreases monotonically again.

This behaviour is expected from the considerations above. Basically we need to compare two timescales, namely the time it takes the small structure to cross the big structure, and the time for a typical orbit in the small structure. The first timescale corresponds to the crossing time for the big structure, which is proportional to our definition of the dynamical time, $\tau_{\rm dyn} = 4r_{\rm s}/v_c(4r_{\rm s})$. The second timescale is similar, but defined for the small structure.

Thus, for a very compact small structure, the particles in the small structure will make many orbits while crossing the big structure, and fewer receive sufficient increase in energy to leave the structure. On the other hand, for a very dilute small structure, the particles in the small structure will perform much less than one orbit while crossing the big structure, rendering the motion almost adiabatic. An extrapolation of this finding is that smooth accretion should not lead to particle ejection.

3 Tracing particles in an analytical potential

In order to demonstrate that the ejection of particles during mergers is a mean field effect, we implement a toy-model in which we consider one particle moving in an analytical time-dependent potential approximating that of the merging structures. In this way we eliminate

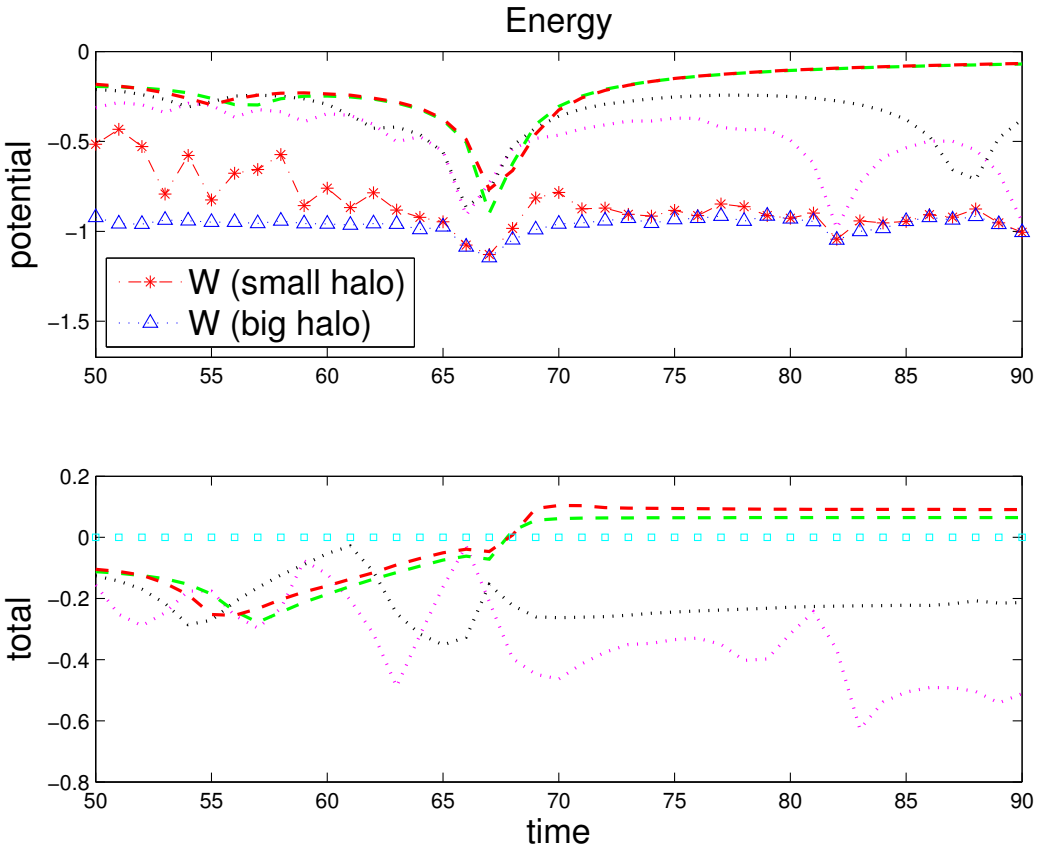

Figure 6. Zoom in on the time variation of potential and total energy. The particles which will remain bound (blue and purple dotted lines) pass through the central region while the potential due to both the small and large structures (symbols) are deepening (around time step 66). This contrasts with the particles which will be ejected (red and green dashed lines), which arrive a little later (time step 67) and pass the centre when the potential is decaying.

dynamical friction entirely. We also eliminate any two-body effects which may be a possible spurious source of particle ejection.

3.1 Simulation Set-Up

We simulate a merger with the same characteristics as the one described in section 2.2.1, but now using a smooth potential instead of the N-body approach used earlier. We then follow the orbits in this potential of a test particle which initially is bound to the small structure[1]. For both structures we use analytical potentials for the same Hernquist model [12]

$$\Phi(r) = -\frac{GM/r_{\rm s}}{1 + r/r_{\rm s}}\,, \tag{3.1}$$

where the large structure has a scale radius $r_{s1} = 1$ and mass $M_1 = 1$, and the smaller one has $r_{s2} = 0.3$ and $M_2 = 0.1$. The two potentials are initially at rest and centered at $15r_{s1}$

[1]This approach is similar to that of [23], but differs in that the latter considered the sum of particles on large orbits (wandering stars) and truly ejected particles. Since we here consider separately the ejected particles (and don't consider the particles merely on large orbits), a direct comparison is not possible.

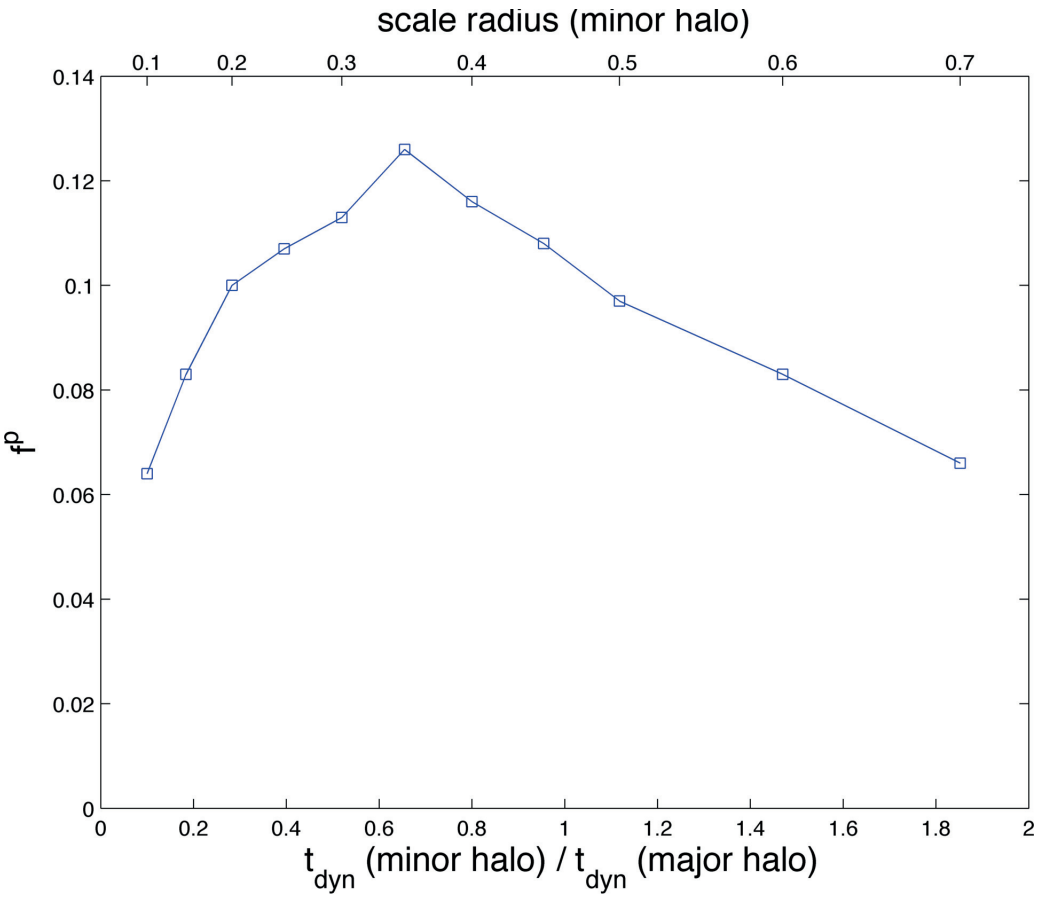

Figure 7. The fraction of particles initially in the small structure which are ejected , f^p, as a function of the ratio between the dynamical times of the small structure and the big structure.

apart along the x-axis, which is the turnaround radius of the big structure, just as discussed in section 2.1. For each time step the potential in which the test particles move is then evolved as follows. The large structure is kept fixed at all times, while the centre of the small structure follows the free fall trajectory induced by the large large structure until the time when their centres coincide. For the subsequent evolution we consider four extreme cases for the interaction between the two potentials, representing extremes between which the full N-body simulation would most likely be.

In the first set of simulations (Case 1) the small structure stops instantaneously when its centre overlaps the centre of the bigger structure; in the second set (Case 2) we let the small structure continue its motion in the x direction, following still its free fall trajectory due to the gravity of the large structure.

In the third and fourth cases, we do as for the first and second cases respectively, but now include a small impact parameter in order to model non-head-on collisions. We achieve this by shifting the velocity direction by hand when the small halo is at $x = 5$.

In each simulation we follow the motion of one particle initially bound to the small potential. We choose its initial position and velocity similarly to how this was done in setting up the N-body simulations, with its radius sampled from the Hernquist mass profile. We assign an initial velocity by determining the typical speed at the radius just chosen, using

an analytical expression for the radial component of the velocity dispersion. We then let the system evolve. For each time step the gravitational attraction of the big structure on the small one, and of both structures on the particle, are calculated using a leapfrog integrator.

3.2 Particle trajectories

In figure 8 we plot the orbits of two different particles, hence two different simulations, belonging to the first set of simulations, in which the potential of the small structure stops (forcing its velocity to zero) when its centre reaches that of the large structure. The red particle is ejected from the system, the blue one remains bounded in the resulting structure and starts orbiting around it.

In figure 9-11 we present similar plots for the other three cases, picking for each case a particle that remains bounded and another that gets ejected.

To get statistics on the particle ejection, we have run 1000 simulations for each case, choosing the test particle randomly as described above. To check for ejection we control the sign and constancy of the total energy of the particle. In the second and in the fourth cases, when the small potential keeps moving in free fall after passing through the big one, it can happen that the particle neither follows the small potential nor gets ejected, but it gets trapped by the bigger potential. If this is the case, the kinetic energy of the particle has to be calculated with respect to the potential of the large structure. We show examples in figures 9 and 11 (in green) of orbits of particles that get bound to the big potential after the collision.

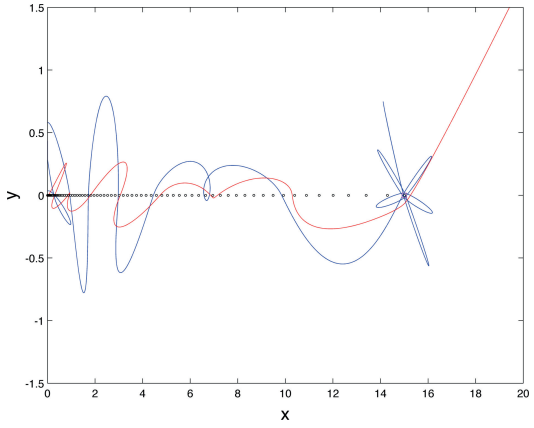

Figure 8. Positions of the centre of the two potentials, and orbits of two particles projected in the spatial coordinates (x, y). Case 1 is a head-on collision where the small potential stops instantaneously as it reaches the big potential, which stays fixed at $x = 15$ and $y = 0$ (magenta square). Black dots are equal time intervals of the positions in x and y of the centre of the small potential. The blue orbit shows a particle that happens to be bound in the final resulting potential, and the red orbit shows a particle that gets ejected from the system.

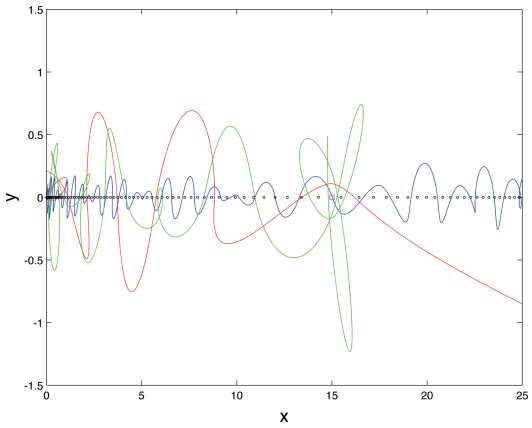

Figure 9. Case 2 is a head-on collision where the small potential continues moving after passing the centre of the big structure. Black dots are equal time intervals of the positions in x and y of the centre of the small potential. The blue orbit shows a particle that happens to be caught in the final resulting potential, and the red orbit shows a particle that gets ejected from the system. The green orbit shows a particle that gets bounded to the larger potential after the merger.

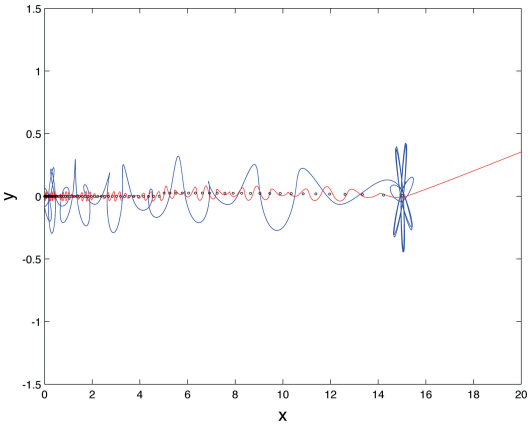

Figure 10. Case 3 is a collision with non-zero impact parameter, where the small potential stops as it reaches the big potential, which stays fixed at $x = 15$ and $y = 0$ (magenta square). Black dots are equal time intervals of the positions in x and y of the centre of the small potential. The blue orbit shows a particle that happens to be caught in the final resulting potential, and the red orbit shows a particle that gets ejected from the system.

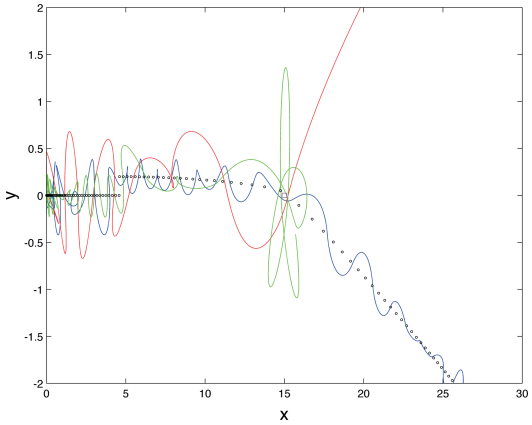

Figure 11. Case 4 is a collision with non-zero impact parameter, where the small potential continues moving after passing the centre of the big structure. Black dots are equal time intervals of the positions in x and y of the centre of the small potential. The blue orbit shows a particle that happens to be caught in the final resulting potential, and the red orbit shows a particle that gets ejected from the system. The green orbit shows a particle that gets bounded to the major potential after the merger.

Table 1. Statistics for particle ejection. 1000 simulations were run for each case. In cases 1 and 3, after the potentials of the small and large structures overlap, the simulation continues only for the test particle, leaving the potentials fixed. In cases 2 and 4 the small potential continues through the large potential, and hence the particle may end up in either of the two, or be ejected.

	Ejected	Small halo	Big halo
Case 1			
Halo stops.	14%	86%	
Head-on.			
Case 2			
Halo doesn't stop.	5.3%	82.4%	12.3%
Head-on.			
Case 3			
Halo stops.	17%	83%	
Impact parameter.			
Case 4			
Halo doesn't stop.	7.2%	76.7%	16.1%
Impact parameter.			

3.3 Fraction of ejected particles

We summarise the results of the 4000 simulations in table 1. For the simulation with the same parameters calculated with the N-body code and described in section 2.2.1, the percentage of the ejected particles is 11%, which lies between the two values of cases 1 and 2.

We notice that in the case of non-head-on collisions the fraction of the mass ejected increases slightly.

4 The relation between scale radius and fraction of ejected particles

We will now study how the fraction of ejected particles from the small structure depends on the size of the minor halo in the merger, and compare the dependence in the N-body simulations with the dependence in simulations, where individual particles are tracked in analytic potentials.

Figure 12 shows the ejected fraction for the head-on mergers for the N-body simulations (from section 2) and the analytical models, where we track particles in an analytic potential (from section 3).

The first thing we notice is that the fraction of ejected particles in the N-body simulations falls within the range spanned by the two analytical models. This result is independent of the scale radius of the minor halo. It is not a surprising result since the way the minor halos evolves in the N-body simulation falls somewhere in between the extreme cases studied in the analytical models, where the minor halo potential is either totally unaffected by the major halo, or it is stopped instantly when it reaches the center of the major halo.

Another result is that the N-body simulation and both analytical models all show a decline in the fraction of ejected particles when the minor halos scale radius is larger than

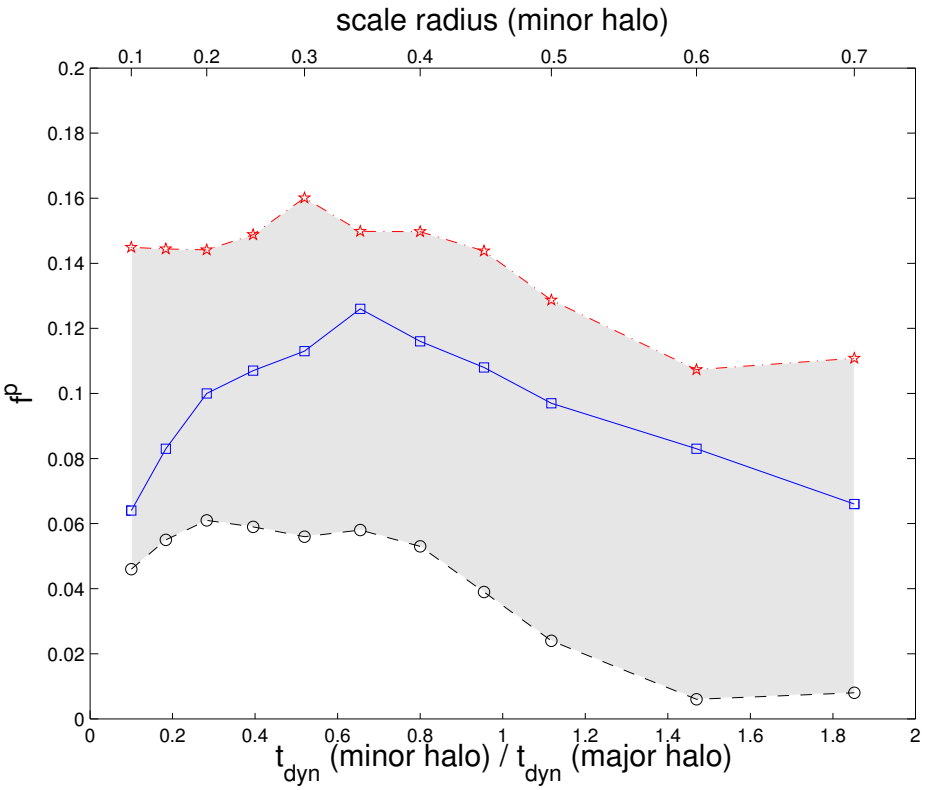

Figure 12. The fraction of ejected particles for the head-on mergers for the N-body simulations (blue), the analytical potential model where the minor halo is stopped when reaching the big one (red dotted), and analytical model where the minor halo continues with free fall velocity through the major halo (black dashed).

$r_{\rm s} \simeq 0.35$ (i.e. 35% of the major halos scale radius). The similarities (the decline in fraction of ejected particles for $r_{\rm s} > 0.35$) and differences (i.e. the different overall normalization in the different models) between the analytical models and the N-body simulations suggest several conclusions

- The detailed destruction history of the minor halo is important for the overall normalisation of the fraction of ejected particles.
- In the setups studied in this work, there is a decline in fraction of ejected particles when the minor halos scale radius reaches 35% of the scale radius of the major halo. This results holds when the mass ratio of the two halos are fixed at 1:10, and will likely change for different mass ratios.
- In the models, where particles are tracked in an analytical potential, dynamical friction between the two merging halos is not present. Because of the similarities between these models and the N-body simulations, we conclude that it is possible to eject particles without dynamical friction. It is still possible that dynamical friction can affect the exact number of ejected particles, but we have shown that it is not the main driver of ejection in minor mergers.

5 Discussion and Conclusion

We have shown that during minor mergers approximately $5 - 15\%$ of the particles from the minor halo are ejected, making the phenomenon quantitatively important in structure formation scenarios. In analytical models (with dynamical friction turned off) and N-body simulations, there exists similar relations between the fraction of ejected particles as a function of the ratio between the scale radii of the two halos in the merger. This similarity shows that dynamical friction is not the driving mechanisms for the ejection of particles.

Instead we find that the relevant mechanism is the increase in the total energy of individual particles arising from the time-dependence of the mean field potential during the merger process. The ejected particles are those that travel in a deep potential as they move in towards the plane of the center of the main halo, and a shallower potential as they move out. In a minor merger these are the particles which originate in the small halo and cross the plane of the center of the large halo slightly later than the center of the halo they originally are bound to does.

In this study we have only considered collisionless systems. It is unclear how the presence of baryons will affect the number of ejected particles. It has been proposed that the potential variations due to supernova feedback can turn galaxy cusps into cores [24, 25], and it is likely that these potential changes can also affect the number of particles ejected during a merger. It is expected that the merging of two galaxies leads to a significant increase in the star formation rate [26], so an increase in the potential variation due to feedback processes is expected during a merger. The exact role of feedback processes will of course depend on the actual feedback model used in the simulation (many different feedback models exist, e.g. [27–30]).

Our finding provides an explanation for the origin of high-velocity component of dark matter particles observed in cosmological N-body simulations. This component of high-velocity particles is important since it potentially may give a clear signature in underground dark matter detectors [8]. This is because particles ejected throughout the merging history of the Universe should permeate space, and also be present in the Earth's neighbourhood, at energies significantly higher than the equilibrated dark matter component. Thus, even though the ejected particles only contribute around 3% of the dark matter near Earth, then they could still induce a peaked signal on top of the broad bump from the thermalized dark matter component.

Acknowledgments

The Dark Cosmology Centre is funded by the Danish National Research Foundation. MJ thanks the Dark Cosmology Centre for financial support as a visitor at the centre.

References

[1] Kazantzidis S., Zentner A. R., Kravtsov A. V., 2006, ApJ, 641, 647

[2] Dehnen, W. 2005, MNRAS, 360, 892

[3] Moore, B. and Kazantzidis, S. and Diemand, J. and Stadel, J., 2004, MNRAS, 354, 522

[4] Sparre M., Hansen S. H., 2012, JCAP, 7, 42

[5] Wojtak, R. and Gottloeber, S. and Klypin, A. 2013, MNRAS, 434, 1576

[6] Valluri M., Vass I. M., Kazantzidis S., Kravtsov A. V., Bohn C. L., 2007, ApJ, 658, 731

[7] Hernquist, L. 1992, ApJ, 400, 460

[8] Behroozi, P. S. and Loeb, A. and Wechsler, R. H. 2013, JCAP, 6, 19

[9] Joyce M., Marcos B., Sylos Labini F., 2009, MNRAS, 397, 775

[10] Springel, V., Yoshida, N. and White, S. D. M. 2001, New Astronomy, 6,79

[11] Springel V., 2005, MNRAS, 364, 1105

[12] Hernquist L., 1990, ApJ, 356, 359

[13] Cuesta A. J., Prada F., Klypin A., Moles M., 2008, MNRAS, 389, 385

[14] Prada F., Klypin A. A., Simonneau E., Betancort-Rijo J., Patiri S., Gottlöber S., Sanchez-Conde M. A., 2006, ApJ, 645, 1001

[15] Macciò A. V., Dutton A. A., van den Bosch F. C., 2008, MNRAS, 391, 1940

[16] Binney, J., & Tremaine, S. 2008, Galactic Dynamics: Second Edition,Princeton, NJ USA, 2008

[17] Hansen, S. H., Juncher, D., & Sparre, M. 2010, ApJ, 718, L68

[18] Sparre M., Hansen S. H., 2012, JCAP, 10, 49

[19] Lynden-Bell D., 1967, MNRAS, 136, 101

[20] Spitzer, L., Jr. 1958, ApJ, 127, 17

[21] Ostriker, J. P., Spitzer, L., Jr., & Chevalier, R. A. 1972, ApJ, 176, L51

[22] Sylos Labini, F., 2013, MNRAS, 429, 679

[23] Teyssier, M., Johnston, K. V., & Shara, M. M. 2009, ApJ, 707, L22

[24] Pontzen, A. & Governato, F. 2013, MNRAS, 421, 3464

[25] Amorisco, N. C., Zavala, J. & de Boer, T. J. L., 2014, ApJ, 782, 39

[26] Hayward, C. C. and Torrey, P. and Springel, V. and Hernquist, L. and Vogelsberger, M., 2013, astroph/1309.2942

[27] Agertz, O. and Kravtsov, A. V. and Leitner, S. N. and Gnedin, N. Y., 2013, ApJ, 770, 25

[28] Vogelsberger, M. et al. 2013, MNRAS436, 3031

[29] Marinacci, F., Pakmor, R. & Springel, V. 2014, MNRAS, 437, 1750

[30] Stinson, G. S. and Brook, C. and Macciò, A. V. and Wadsley, J. and Quinn, T. R. and Couchman, H. M. P. 2013, MNRAS, 428, 129